Sensors and Materials, Vol. 36, No. 7 (2024) 2669–2683
MYU Tokyo

S & M 3694

Characteristics of Displacement Behavior of Dummy Skin Using Convergent Ultrasonic Haptic Actuators

Daisuke Mizushima[1*] and Nobuya Sato[2]

[1]Department of Electrical and Electronics Engineering, Aichi Institute of Technology,
1247 Yachigusa, Yakusa, Toyota City, Aichi 470-0392, Japan
[2]Department of Applied Chemistry, Aichi Institute of Technology,
1247 Yachigusa, Yakusa, Toyota City, Aichi 470-0392, Japan

(Received March 28, 2024; accepted June 25, 2024)

Keywords: haptics, biosensing, human skin, laser displacement meter, tactile sensation

Haptics is a research field related to the sense of touch. When humans perceive vibrations, the magnitude of sensory quantity is determined by the amount of skin displacement. A haptic actuator using mid-air ultrasonic waves is suitable for measuring the skin displacement during tactile presentation because they allow contactless tactile presentation. However, studies that directly observe the amount of skin displacement during the sensing of vibration have been conducted only at a very limited displacement of 3 μm, despite the sensible skin displacement range being approximately 10 mm–0.01 μm. In this study, ultrasonic speakers were used to generate higher sound pressures than conventional ultrasonic speakers to produce large displacements. The goals of this study are to observe the characteristics of skin displacement and to map the amount of displacement to the sensory amount. In this paper, we used a dummy skin instead of a biological skin to investigate the validity of the constructed observation system and the adaptability of the skin viscoelasticity model proposed in the previous study. From the measurement results, obtained at a maximum acoustic radiation pressure of 4000 Pa, a maximum displacement of 170 μm is obtained. This is 50 times larger than that obtained in the previous study. The displacement amount is consistent with the displacement model proposed in the previous study and the elastic modulus obtained from the dynamic viscoelasticity measurement. Furthermore, the simulation results obtained from that model suggest that the displacement characteristics of Asker C15 of HITOHADA® GEL would be similar, suggesting that this HITOHADA® GEL could be used as an alternative material.

1. Introduction

Haptics is a research field related to the sense of touch. It is attracting attention as the third sensory engineering following vision and hearing, and it has been actively researched in recent years. It encompasses various facets of an object and can be conveyed as information through tactile sensation. This includes attributes such as hardness, softness, roughness, dryness, and wetness. It is believed that these types of information can be effectively transmitted using an

*Corresponding author: e-mail: d-mizushima@aitech.ac.jp
https://doi.org/10.18494/SAM5054

ISSN 0914-4935
https://myukk.org/

appropriate combination of sensors and actuators. If such tactile transmission technology is realized, tactile information about an object can be obtained without physically touching the object, thereby reducing the need for people and objects to move. Until now, haptics has primarily found its applications in the entertainment field. However, with the global spread of infectious diseases and growing environmental consciousness, there is a growing interest in utilizing haptics in the medical and industrial sectors.[1–3]

Haptics is a multidisciplinary field including physiology and electrical and materials engineering. In the development of sensory technologies, the physiological knowledge about the involved physical quantities, receptors, and threshold values for stimulus generation is indispensable. In the field of haptics, these insights have been elucidated through previous research studies. For example, it has been found that there are four types of mechanoreceptor—Merkel cells, Meissner corpuscles, Ruffini endings, and Pacinian corpuscles—located beneath the human skin. These receptors transmit tactile stimulation to the nervous system in response to vibrations caused by external factors.[4,5] The threshold skin displacement values at which these receptors generate tactile stimulation have also been experimentally determined.[6]

Combining these physiological insights, the theory of tactile primary colors has been proposed by Inoue *et al.*[7] According to this theory, just as in vision, in which various colors are expressed through the combination of the three colors red, green, and blue, in tactile perception, various tactile sensations are considered to be generated through the combination of three physical quantities, force, vibration, and temperature. Actuators based on this theory have been developed. Reports indicate that presenting all three physical quantities simultaneously improves the realism of tactile sensations as compared with presenting force or vibration alone.[8] The tactile primary color theory is the most plausible theory for explaining the physiological mechanisms of touch.

On the engineering side of haptics, various types of actuator for providing tactile sensations have been developed. Vibration actuators that utilize eccentric motors were developed long ago and have been incorporated into devices such as game controllers.[9] In addition, various actuators have been devised, including those that use piezoelectric elements,[10] those based on the resonance structure of vibrating bodies,[11] and those utilizing shape memory alloy.[12] Among such actuators, the authors are interested in actuators that use convergent ultrasonic. These actuators utilize convergent ultrasonic waves in an arbitrary space to generate acoustic radiation pressure, which pushes the skin into the actuators.[13]

Currently, these actuators are evaluated on the basis of factors such as the magnitudes of generated acceleration and vibration. However, as mentioned above, the magnitude of tactile sensation is related to that of displacement occurring in the skin, and it is not fully understood how these actuators affect the displacement behavior of the skin.

There were previous studies that addressed these issues by quantifying skin displacement. The skin displacements during the presentation of tactile sensations were observed by Chilles *et al.*[14] and Frier *et al.*[15] Such observation was conducted using a laser Doppler displacement meter and an actuator that employs converging ultrasonic waves. However, the skin displacements obtained in these experiments are very small, only 3 μm. The vibration frequency was measured at a specific value. Since the maximum amount of skin displacement is 1–10 mm,

it is difficult to say that they cover the dynamic range of displacement that is the target of haptics.

Mizushima and Sato focused on this point and developed an ultrasonic haptics actuator that is smaller than those in previous studies. An acoustic radiation pressure higher than that used in previous studies was generated by converging ultrasonic waves over a very short distance.[16] This research aims to address the challenge of visualizing and quantifying the displacement behavior of the skin using this actuator. This study extends the design principle of this actuator by using an ultrasonic speaker, which produces a stronger acoustic pressure than conventional actuators, to construct a small actuator. The combination of these actuators generates approximately twice the acoustic radiation pressure compared with the previous study and addresses the issue of visualizing skin displacement behavior. The goal is to observe the behavior of the biological skin, but observing a living body is difficult. Therefore, in this study, a polymer dummy skin that mimics skin from a materials engineering perspective is used. The displacement behavior of the dummy skin was confirmed, and the model proposed in previous studies was extended to wide ranges of frequencies and displacements to confirm its suitability. Furthermore, by comparing the viscoelasticity of the dummy skin with that of the actual skin, alternative materials that can simulate the displacement behavior of the biological skin were considered.

2. Principles and Methods

2.1 Tactile receptors

As mentioned earlier, four types of mechanoreceptor are present beneath the human skin. These mechanoreceptors are classified according to the reaction time and the depth of their location under the skin. Merkel cells respond slowly and are present in shallow locations [slow adaption I (SA I)]. Meissner corpuscles respond rapidly and are present in shallow locations [fast adaption I (FA I)]. Ruffini endings respond slowly and are present in deep locations [slow adaption II (SA II)]. Pacinian corpuscles respond rapidly and are present in deep locations [fast adaption II (FA II)]. These receptors receive stimuli, such as pressure on the skin or skin curvature, and transmit tactile sensations to the nervous system. Each of these receptors has a different threshold and detection frequency band.[17] The haptic three-primary color theory summarizes how stimuli transmitted from mechanoreceptors to nerves combine to lead to tactile sensations. An overview of this three-primary color theory is shown in Fig. 1. According to this theory, the combination of three physical quantities (force, vibration, and temperature) is considered to produce various tactile sensations. This is an important theory that can serve as a guideline for the development of sensors and actuators for haptics.[7]

The detection thresholds for the haptic three primary colors are already known. Force, in terms of pressure, is 2 mg/mm^2 at the most sensitive point. As for temperature, both coldness and warmth can be detected with a change of 0.5 K per 0.1 s.[18,19] The frequency variation of this threshold has been experimentally summarized by Bolanowski *et al.*,[6] whose results are shown in Fig. 2, which indicates that the vibration frequency detectable by the human skin ranges from 0.4 to 600 Hz.

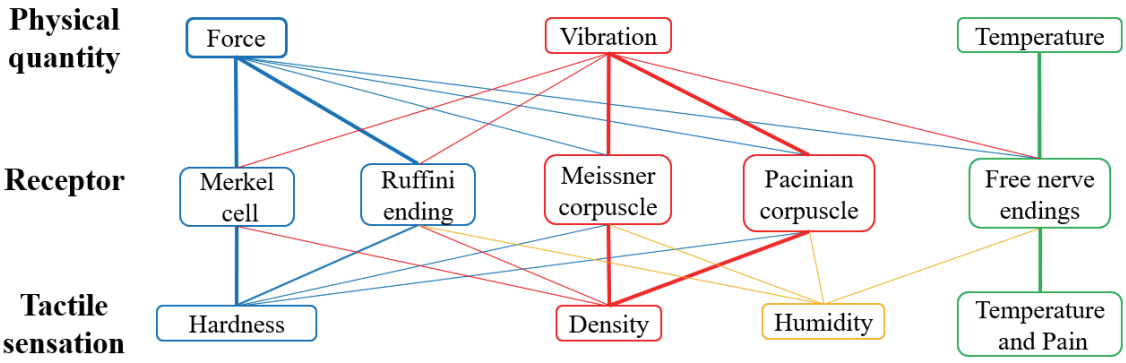

Fig. 1. (Color online) Overview of three-primary color theory.[7]

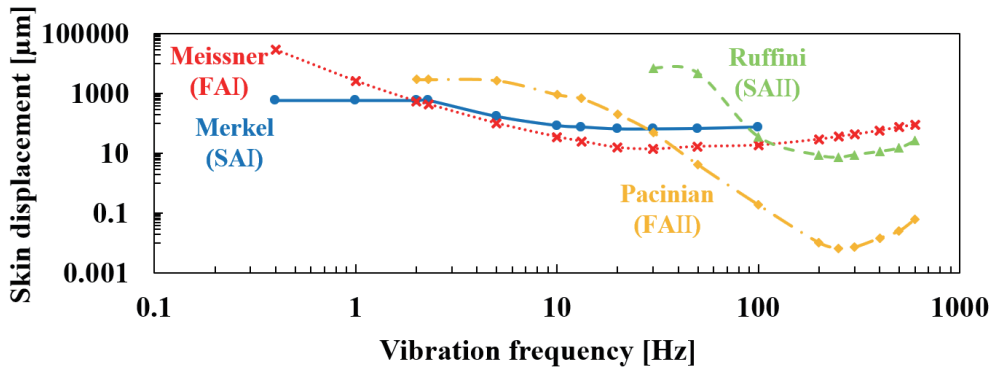

Fig. 2. (Color online) Vibration frequency characteristics of threshold skin displacement.[2]

2.2 Mechanical model of skin displacement

The skin displacement due to convergent ultrasonic waves has been modeled by Chilles *et al.*[14] The model is the standard linear solid model (SLSM) shown in Fig. 3. In Fig. 3, σ is the stress applied to this model and ε is the strain of this model. As strain ε represents the ratio of displacement to thickness, the actual displacement magnitude is calculated by multiplying the strain by the skin thickness. E_1, E_2, and η_3 represent the elastic modulus at a low frequency, the elastic modulus at a high frequency, and the viscosity at a high frequency, respectively. The values of E_1, E_2, and η_3 can be obtained from dynamic viscoelasticity test results. The storage modulus obtained from a dynamic viscoelasticity test is E' and the loss modulus is E''; the relationship between these moduli and viscosity is as follows.[20]

$$E' = \frac{E_1 {E_2}^2 + \omega^2 {\eta_3}^2 \left(E_1 + E_2\right)}{{E_2}^2 + \omega^2 {\eta_3}^2} \tag{1}$$

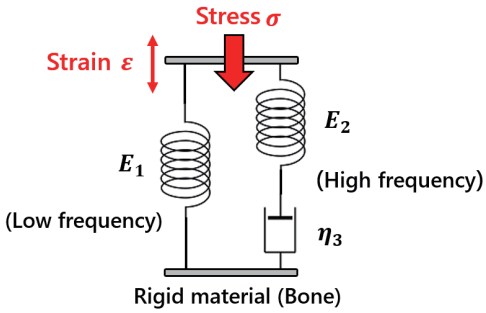

Fig. 3. (Color online) Mechanical model of skin (SLSM).

$$E'' = \frac{\omega \eta_3 {E_2}^2}{{E_2}^2 + \omega^2 {\eta_3}^2} \tag{2}$$

Here, ω is the angular frequency of excitation in a dynamic viscoelasticity test. The relationship between stress and strain in SLSM is expressed as

$$\sigma + \frac{\eta_3}{E_2}\frac{\mathrm{d}\sigma}{\mathrm{d}t} = E_1\varepsilon + \frac{\eta_3\left(E_1 + E_2\right)}{E_2}\frac{\mathrm{d}\varepsilon}{\mathrm{d}t}, \tag{3}$$

where the first term on both sides represents the displacement in response to quasi-static stress. When stress is applied to a material by ultrasonic, a quasi-static displacement occurs. If the frequency of the applied ultrasonic wave is f, the elastic modulus at low frequencies is replaced by the equivalent elastic modulus E_d as shown in Eq. (4).

$$E_d = \frac{\left(E_1E_2\right) + \eta_3 f\left(E_1 + E_2\right)}{E_2 + \eta_3 f} \tag{4}$$

Thus, Eq. (3) can be replaced by Eq. (5).

$$\sigma + \frac{\eta_3}{E_2}\frac{\mathrm{d}\sigma}{\mathrm{d}t} = E_d\varepsilon + \frac{\eta_3\left(E_d + E_2\right)}{E_2}\frac{\mathrm{d}\varepsilon}{\mathrm{d}t} \tag{5}$$

In this paper, amplitude modulation is applied to the convergent ultrasonic wave to generate sensible vibrations in the skin. Therefore, the obtained vibration displacement is expressed by the following Eq. (6), neglecting the quasi-static term on both sides of Eq. (5).

$$\sigma = \left(E_d + E_2\right)\varepsilon \tag{6}$$

2.3 Generation of acoustic radiation pressure

When an actuator using convergent ultrasonic waves causes skin displacement, the force applied to the skin is the acoustic radiation pressure due to ultrasonic waves. It corresponds to the stress σ in Fig. 3 and Eq. (6). Figure 4 presents an overview of the ultrasonic actuator used to focus the ultrasonic waves during the experiment. The actuator has six speakers arranged so that the surfaces of the speakers are aligned on a parabola with the focal length set to an arbitrary value. Ideally, the speakers are spaced on the parabola at a distance equal to the diameter of the speaker. The origin is the midpoint between speakers 3 and 4. If the distance from the origin is r, the sound pressure p radiating from the ultrasonic speakers is calculated using the Rayleigh equation as follows:

$$p = \rho c V \left[\exp(-jkr) - \exp\left(-jk\sqrt{a^2 + r^2}\right) \right]. \tag{7}$$

In Eq. (7), ρ is the density of air, c is the speed of sound waves in the air, V represents the amplitude of the diaphragm inside the speaker and is proportional to the input voltage, and $k = 2\pi f/c$. Here, a denotes the diameter of the diaphragm, and the speaker diameter is usually larger than a. According to Eq. (7), the sound pressure oscillates in the near field, where the distance from the sound source is small and close, and the sound pressure is inversely proportional to the distance in the far field. The boundary distance between the two is the Rayleigh length, denoted as Z_0.

$$Z_0 = \frac{a^2}{2k} \tag{8}$$

In the ultrasonic speaker used in this study, where the speaker diameter is 10 mm, $a = 6$ mm, and $f = 40$ kHz, and considering the speed of sound $c = 343$ m/s in air at an ambient temperature, the Rayleigh length is approximately 10 mm. The angle of each speaker to the focal point is approximately 40° for speakers 1 and 6, 28° for speakers 2 and 5, or 10° for speakers 3 and 4, assuming that the line connecting the origin and the focal point is 0°. If the sound pressure

Fig. 4. (Color online) Overview of ultrasonic actuator.[18]

radiating from each loudspeaker is denoted as p_i, the total sound pressure p_{total} is expressed as follows when the ultrasonic waves are focused from the six speakers:

$$p_{total} = \sum_{i}^{6} p_i \sin\left(2\pi ft + \theta_i\right). \tag{9}$$

Note that θ_i represents the phase difference at the focus of the ultrasonic waves generated by each speaker. The acoustic radiation pressure P is expressed as

$$P = \alpha \frac{{p_{total}}^2}{\rho c^2}, \tag{10}$$

where α is a constant that represents the absorption and reflection of sound waves. From Eq. (10), it can be seen that the acoustic radiation pressure is proportional to the square of the sound pressure p_{total} and to the square of the input voltage.

3. Experimental Setup

The ultrasonic speakers used have a resonance frequency of about 40 kHz, but the detectable frequency of haptic vibration ranges from 0.4 to 600 Hz. 40 kHz signals are used as carrier waves, and amplitude modulation (AM) is applied to produce vibrations of detectable frequency. The ultrasonic speaker used was SE-40A1 (TAMURA Co., Ltd.), known for its ability to produce higher sound pressure levels than general-purpose ultrasonic speakers. For displacement measurement, a Keyence LK-G30 laser displacement meter, which has a high repeatability of 0.05 μm and measures the diffuse reflection from a rough surface, is used because it is considered suitable for this experiment.

The experimental setups of this study are shown in Figs. 5(a)–5(c). The system for the measurement of the acoustic radiation pressure obtained from the actuators is shown in Fig. 5(a). Two actuators with a focal length of 50 mm are used and installed at an angle of 30° to the laser optical axis so that the laser beam length is focused at 30 mm, the standard measurement distance for the LK-G30. Figure 5(b) shows a photograph of the actuator alongside the setup of the laser displacement meter. The amplitude modulated sine waves with an arbitrary modulation frequency, modulation factor, and input voltage are generated by a function generator, amplified by a DENON amplifier (PMA-600), and input to the actuators. A Brüel & Kjær Type 4938 microphone is used as the measurement microphone. The output from the microphone is amplified by a Brüel & Kjær Type 2690 conditioning amplifier to measure the magnitude of acoustic radiation pressure with an oscilloscope. The distance between the microphone and the laser displacement meter surface is used as a parameter in the measurement. The displacement measurement system of the dummy skin using an ultrasonic haptics actuator is shown in Fig. 5(c). The configuration and layout of the actuator are the same as that shown in Fig. 5(a).

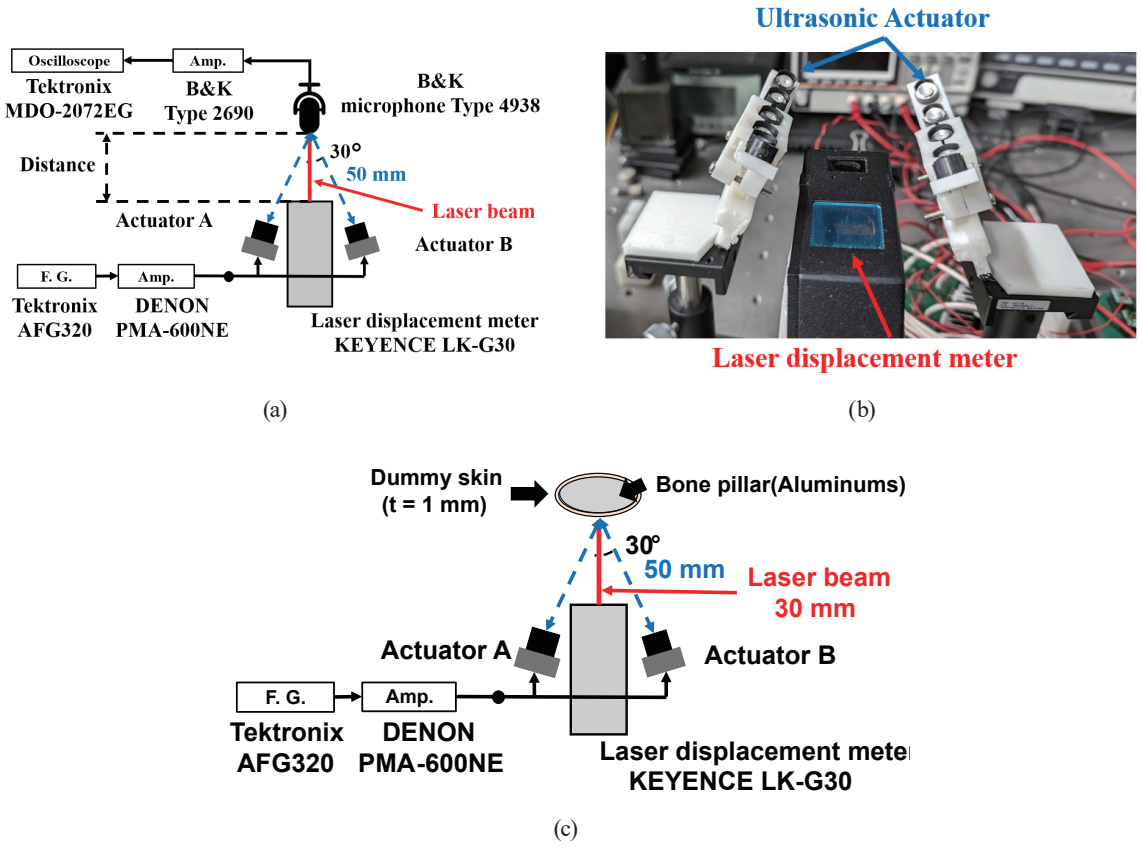

Fig. 5. (Color online) Experimental setup: (a) acoustic pressure measurement system, (b) picture of actuator and laser displacement meter, and (c) displacement measurement system.

The dummy skin used was HITOHADA® GEL (EXSEAL Co., Ltd.). The HITOHADA® GEL was manufactured to a thickness of 1 mm and then cut into squares measuring 50 × 50 mm^2. Three different Asker C hardnesses of the HITOHADA® GEL were used: 0, 7, and 15 (JIS K 7312). The HITOHADA® GEL was wrapped around an aluminum bone, which resembled the bone of the human index finger, and placed 30 mm away from the surface of the laser displacement meter. When the HITOHADA® GEL was repeatedly compressed and stretched perpendicularly to its surface, the measured frequency characteristics (master curves) of dynamic viscoelasticity are as shown in Figs. 6(a)–6(d). Figure 6(a) shows the measurement system. When the skin is vibrated by an acoustic radiation pressure, a compressive force is applied with a certain periodicity perpendicular to the skin surface. Therefore, the measurement is in the compression mode, in which the material is clamped by a jig and vibrated. RSA3 from TA Instruments Inc. was used for the measurement, for which a sample is cut into a 2-mm-diameter circle and a dynamic strain of 10% was applied perpendicularly to the surface at a constant period. The frequency range of obtained data is 0.1 Hz–1 MHz; however, in this paper, we include the measurement results from 1 to 1000 Hz, which are important for haptics applications. Figures 6(b)–6(d) show the measured viscoelasticities of Asker C0, C7, and C15,

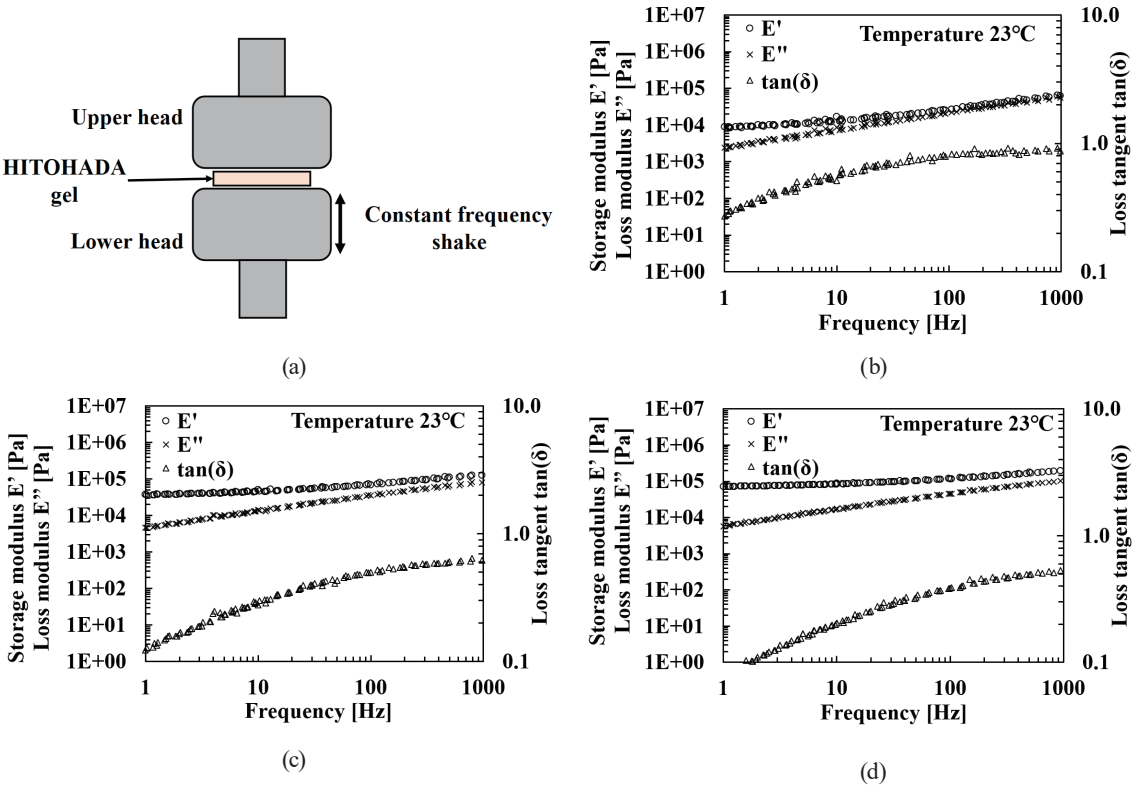

Fig. 6. (Color online) (a) Experimental setup of viscoelasticity measurement of (b) Asker C0, (c) Asker C7, and (d) Asker C15.

respectively. E' is the storage modulus representing elasticity, E'' is the loss modulus representing viscosity, and loss tangent (tan δ) is the ratio of the loss modulus to the storage modulus. From the measurement results, the storage modulus was found to be proportional to the vibration frequency for all materials. The loss modulus is similar for all materials, but the storage modulus is proportional to hardness. For example, the storage modulus of Asker C0 is 1.07×10^4 Pa, that of Asker C7 is 5.08×10^4 Pa, and that of Asker C15 is 8.35×10^4 Pa at 10 Hz. Since the compressive modulus of the human skin is about 1.34×10^5 Pa, the storage modulus of the HITOHADA® GEL is slightly lower than that of the human skin, but considered comparable.[20–22] The loss tangents increased from 1 to 100 Hz, but almost saturated to a constant value above 100 Hz. This result suggests that a stable viscous behavior is exhibited above 100 Hz.

4. Characteristics of Acoustic Radiation Pressure

A 40 kHz carrier wave is beyond the skin detection band, so it is perceived as static pressure, not vibration. Thus, the modulation frequency component of the acoustic radiation pressure is important for haptics. Therefore, in this section, we present the measured modulation frequency component of the acoustic radiation pressure. According to the configuration shown in Fig. 5(a), where the room temperature is 23 ℃ and the distance between the surface of the laser

displacement meter and the measurement microphone is 30 mm, the modulation frequency component of acoustic radiation pressure generated by the actuator was measured, and the results are shown in Figs. 7(a)–7(c). Thereafter, all the measured values presented indicate the average of five measurements. When the modulation frequency and factor are constant, the modulation frequency component of the acoustic radiation pressure is proportional to the square of input voltage as shown in Fig. 7(a). It is considered that the generated sound pressure of each ultrasonic speaker is proportional to the input voltage, so the acoustic radiation pressure is proportional to the square of the input voltage as shown in Eq. (10). When the modulation frequency and input voltage are constant, the modulation frequency component of acoustic radiation pressure is proportional to the modulation factor as shown in Fig. 7(b). When the input voltage is constant, the radiation pressure generated by the carrier wave is constant. With decreasing modulation factor, the modulation frequency component of acoustic radiation pressure decreases and the static radiation pressure increases. When the modulation factor and input voltage are constant versus the modulation frequency, the modulation frequency component of acoustic radiation pressure slightly decreases above 300 Hz as shown in Fig. 7(c). This is due to the resonant characteristics of the piezoelectric elements in ultrasonic speakers. In this type of actuator, the carrier frequency is varied by modulation. When the modulation frequency increases beyond a certain level, the signal frequency is beyond the peak of resonance and the radiation efficiency decreases.

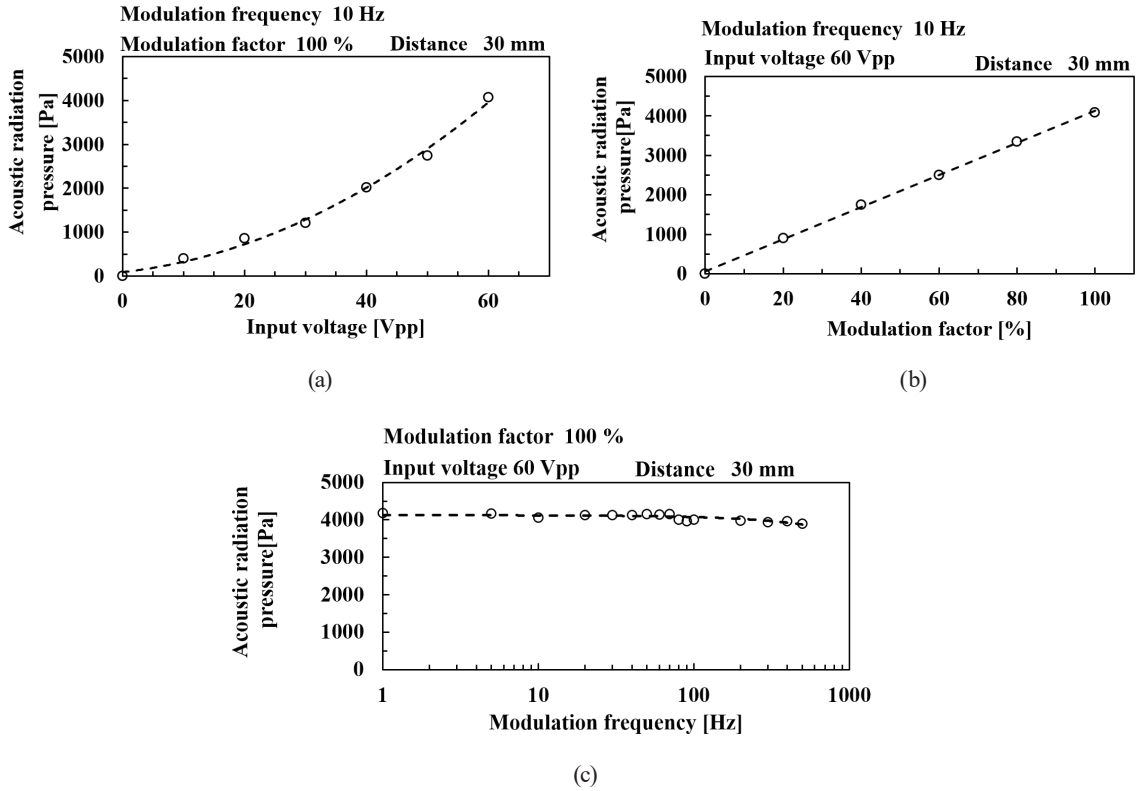

Fig. 7. Measured acoustic radiation pressure versus (a) input voltage, (b) modulation factor, and (c) modulation frequency.

Next, the microphone was moved in the same configuration as in Fig. 7, and the half-width of the acoustic radiation pressure was measured. An actuator consisting of multiple ultrasonic speakers has a focal point where the radiation pressure is maximum. As a quantitative indicator of the focal point size, the width at half maximum is shown. The width at half maximum of the acoustic radiation pressure can be a parameter that indicates the range within which tactile sensation can be felt. The measurement results are shown in Fig. 8. When the modulation frequency, modulation factor, and input voltage were constant, the acoustic radiation pressure peaked at 30 mm and showed a sharp rise and a gradual fall versus the distance from the laser displacement meter surface to the microphone as shown in Fig. 7(a). This result indicates that the focal point is formed at the assumed location. The half-width of the acoustic radiation pressure is approximately 8 mm on one side. This is appropriate since the wavelength of 40 kHz ultrasonic waves is 8.6 mm at room temperature. With respect to the acoustic pressure distribution of the modulation frequency component of acoustic radiation pressure at the focal plane as shown in Fig. 7(b), the half-width of the acoustic radiation pressure in the *x*-direction is approximately 10 mm on one side and that in the *y*-direction is approximately 3 mm on one side. Since the ultrasonic speakers are aligned along the *y*-direction in the figure as the longitudinal direction, the half-width in the *x*-axis direction is larger than that in the *y*-axis direction. The focal point size did not change significantly with changes in modulation frequency, modulation factor, or input voltage.

5. Displacement Characteristics of Dummy Skin

According to the configuration shown in Fig. 5(c), where the room temperature is 23 °C and the distance between the surface of the laser displacement meter and the dummy skin is 30 mm, the displacement amounts were measured by the laser displacement meter and the results are shown in Figs. 9(a)–9(c). In Figs. 9(a)–9(c), the dotted and dashed lines are the theoretical values of the displacements calculated using Eq. (6). Circles, diamonds, and triangles indicate the average of five measured displacements, and error bars indicate their maximum and minimum measured values.

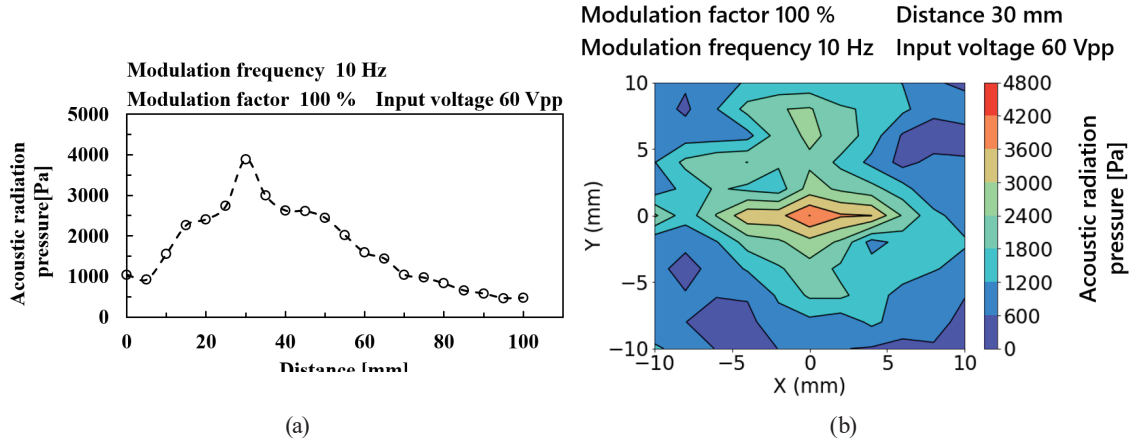

(a) (b)

Fig. 8. (Color online) Measured acoustic radiation pressure distribution versus (a) distance from displacement meter and (b) pressure distribution on focal plane.

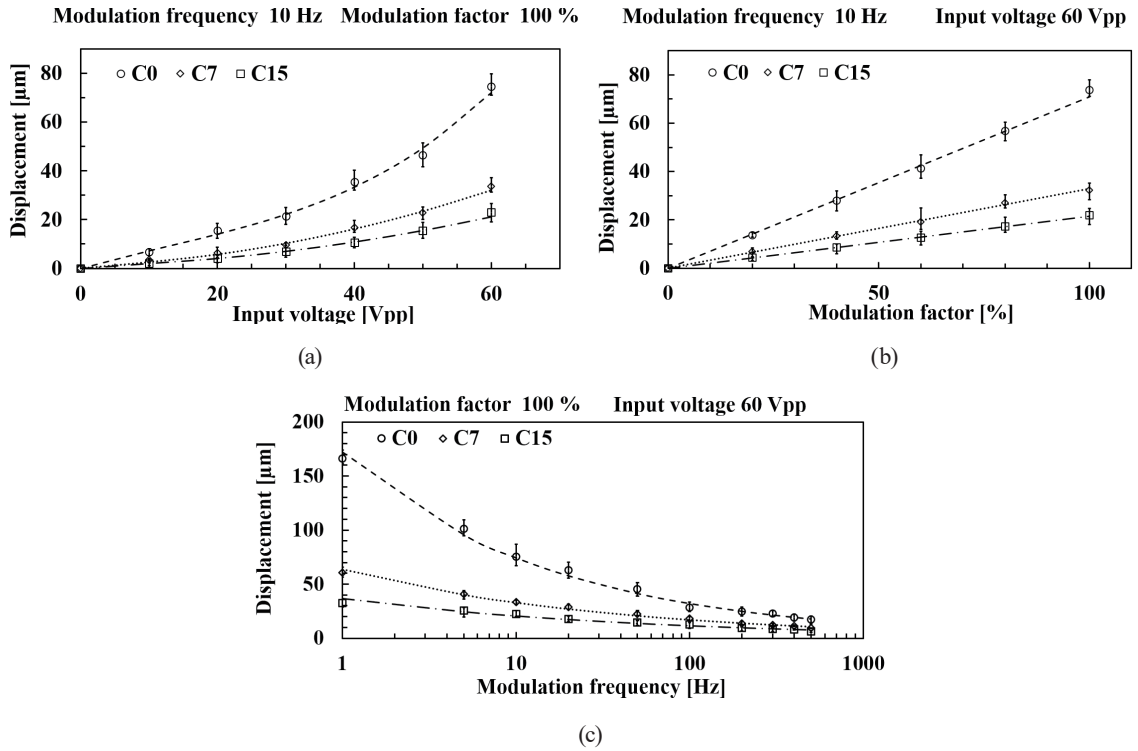

Fig. 9. Measured displacement versus (a) input voltage, (b) modulation factor, and (c) modulation frequency.

When the modulation frequency and factor are constant, the measured displacement amounts versus the input voltage show the same trend as the theoretical curve as shown in Fig. 9(a). The measured and theoretical values fall within the range indicated by the error bars. In comparison with the characteristics shown in Fig. 7(a), the variation of acoustic radiation pressure is proportional to the square of the input voltage, and the variation of acoustic radiation pressure is proportional to the amount of displacement. When the modulation frequency and input voltage are constant, the displacement amount is proportional to the modulation frequency component of acoustic radiation pressure versus the modulation factor as shown in Fig. 9(b), as compared with the characteristics shown in Fig. 7(b). In addition, the measured values and theoretical curves generally show the same trend in this characteristic, and the theoretical values fall within the range indicated by the error bars. From these characteristics, it is indicated that the displacement variation due to the acoustic radiation pressure variation was measured correctly. When the modulation factor and input voltage are constant, a maximum displacement of 170 μm is observed versus the modulation frequency as shown in Fig. 9(c), and the theoretical curve and measured values show a similar trend in this characteristic. Since the acoustic radiation pressure does not change with the modulation frequency, the frequency characteristics of displacement amount can be attributed to the viscoelasticity of the dummy skin. The measurement results are consistent with the theoretical value of the displacement of the SLSM obtained from the dynamic viscoelasticity test results. Therefore, it can be considered that the behavior of the skin model

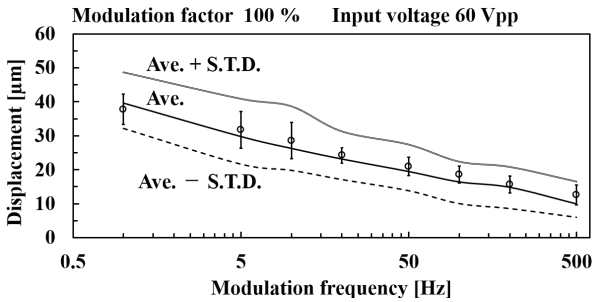

Fig. 10. Measured displacement of Asker C15 versus simulated displacement of human finger skin.

shown in a previous study can be reproduced and that the proposed method can correctly measure the displacement.

In this experiment, the compressive modulus of the human skin was utilized, despite the presence of several literature values for its elasticity. The compressive modulus was determined experimentally to be approximately 1 Hz by Nishio *et al.* and in the range of 100–1000 Hz by Kearney *et al.*[20,21] Using these literature values, we simulated the displacement characteristics of the human finger skin using Eq. (6). Figure 10 illustrates a comparison between the simulation results and the displacement property results for Asker C15. The markers in the figure represent the actual measured values of Asker C15 along with their standard deviations. The solid line shows the displacement simulated by adopting the average viscoelasticity obtained from the literature, whereas the double line represents the displacement simulated by adding the standard deviation to the average viscoelasticity. The dashed line shows the displacement simulated by subtracting the standard deviation from the average viscoelasticity. All measured values fell within the range of the maximum and minimum values, suggesting that the human skin gel Asker C15 may be capable of simulating the displacement characteristics of the human finger skin.

6. Conclusions

In haptics, actuators that present tactile sensations are evaluated in terms of the magnitudes of generated acceleration and vibration. However, the magnitude of tactile sensation is related to the displacement amount of the skin, and this is not well understood. In this study, we focused on this point and addressed the issue of visualization and quantification of skin displacement behavior using an ultrasonic haptics actuator that is smaller than those in previous studies. The purpose of this study is to observe the displacement of the human skin, but observing a living body is difficult. Therefore, in this study, we observe the displacement behavior using a polymeric material that simulates the skin and confirm its consistency with existing materials engineering theories.

By using a small bow-shaped actuator with high focal point accuracy, a maximum acoustic radiation pressure of approximately 4000 Pa could be obtained from 12 ultrasonic speakers. The half-width of the acoustic pressure at the focal point was determined to be 3 mm per side for the

longitudinal direction (*y*-direction), 8 mm per side for the shortitudinal direction (*x*-direction), and 10 mm for the direction parallel to the laser beam (*z*-direction) of the bow-shaped actuator. This size is considered reasonable since the frequency of the ultrasonic wave used as the carrier wave is 40 kHz and the wavelength in air at room temperature is 8.5 mm.

Using the aforementioned actuator, we measured the displacement of a dummy skin with viscoelasticity comparable to that of a real skin. We were able to measure displacements in the range of 1–500 Hz, with a maximum displacement of 170 μm observed. In contrast to a previous study, which examined frequencies of 50 and 200 Hz with a maximum displacement of approximately 3 μm, our study confirmed displacement over a much broader frequency range. The results align with both the displacement model proposed in the previous study and the findings derived from dynamic viscoelasticity measurements. Furthermore, the simulation results obtained from the model suggest that the displacement characteristics of Asker C15 are similar to those of the human skin gel, suggesting that the human skin gel could be a vital alternative material.

Acknowledgments

We would like to express our sincere gratitude to the Chemical Evaluation Research Institute (CERI) for assistance in the viscoelastic measurements.

References

1 K. Tadano, W. Sumino, and K. Kawashima: J. Rob. Soc. Jpn. **27** (2009) 538. https://doi.org/10.7210/jrsj.27.538
2 K. Ohnishi and T. Mizoguchi: IEEJ Trans. Electr. Electron. Eng. **12** (2017) 803. https://doi.org/10.1002/tee.22562
3 T. Nozaki and S. Hangai: J. Rob. Soc. Jpn. **36** (2018) 668. https://doi.org/10.7210/jrsj.36.668
4 M. Tanaka: Int. J. Jpn. Soc. Precis. Eng. **82** (2016) 20. https://doi.org/10.2493/jjspe.82.20
5 M. Nakatani: Syst. Control Inf. **64** (2020) 126. https://doi.org/10.11509/isciesci.64.4_126
6 S. J. Bolanowski, G. A. Gesheider, R. T. Verrillo, and C. M. Checkosky: J. Acoust. Soc. Am. **84** (1988) 1680. https://doi.org/10.1121/1.397184
7 Y. Inoue, I. Naka, F. Kato, and S. Tachi: Trans. Virtual Reality Soc. Jpn. **25** (2020) 86. https://doi.org/10.18974/tvrsj.25.1_86
8 Y. Tajima, F. Kato, Y. Inoue, and S. Tachi: Trans. Virtual Reality Soc. Jpn. **24** (2019) 125. https://doi.org/10.18974/tvrsj.24.1_125
9 V. Yem, R. Okazaki, and H. Kajimoto: Trans. Virtual Reality Soc. Jpn. **21** (2016) 555. https://doi.org/10.18974/tvrsj.21.4_555
10 L. Song, S. Glinsek, S. Dmovsek, V. Kovacova, B. Malic, and E. Defay: Appl. Phys. Lett. **121** (2022) 212901. https://doi.org/10.1063/5.0106174
11 K. Tanabe, S. Takei, and H. Kajimoto: Proc. Entertainment Computing 2015 (Information Processing Society of Japan 2015) 2A1-B07(1). https://doi.org/10.1299/jsmermd.2015._2A1-B07_1
12 G. Chernyshov, B. Tag, C. Caremel, F. Cao, G. Liu, and K. Kunze: Proc. 2018 ACM Int. Symp. Wearable Computers (Association for Computing Machinery, New York, 2018) 112–119. https://doi.org/10.1145/3267242.3267257
13 R. Takahashi, K. Hasegawa, and H. Shinoda: IEEE Trans. Haptics **13** (2020) 334.
14 J. Chilles, W. Frier, A. Abdouni, M. Giordano, and O. Georgiou: Proc. 2019 IEEE World Haptics Conf. (IEEE, 2019) 259. https://doi.org/10.1109/WHC.2019.8816097
15 W. Frier, A. Abdouni, D. Pittera, O. Georgiou, and R. Malkin: IEEE Access **10** (2022) 15443. https://doi.org/10.1109/ACCESS.2022.3147725
16 D. Mizushima and D. Sato: Sensing Technology: Proc. Int. Conf. Sensing Technology 2022 (Springer, Heidelberg, 2023) 267. https://doi.org/10.1007/978-3-031-29871-4_27

17 Y. Shimizu: Jpn. J. Ergonomics **24** (1988) 157. https://doi.org/10.5100/jje.24.157
18 A. Chikada: Trans. J. Textile Mac. Soc. Jpn. **45** (1992) 189. https://doi.org/10.4188/transjtmsj.45.4_P189
19 K. Doi, T. Nishimura, A. Seo, K. Kushiyama, and T. Baba: Trans. Jpn. Soc. Kansei Eng. **11** (2012) 419. https://doi.org/10.5057/jjske.11.419
20 S. P. Kearney, A. Khan, Z. Dai, and T. J. Royston: Phys. Med. Biol. **60** (2015) 6975. https://doi.org/10.1088/0031-9155/60/17/6975
21 Y. Nishio, Y. Ito, R. Nishida, Y. Kagiyama, and T. Nemoto: J. Jpn. Soc. Exp. Mech. **16** (2017) 307. https://doi.org/10.11395/jjsem.16.307
22 K. Yamaba, H. Kono, and S. Ozaki: Biomechanisms **3** (1975) 27. https://doi.org/10.3951/biomechanisms.3.27